2010

Full tensor diffucion is not required to access the white-matter integrity in mouse contusion spinal cord injury

Tsang-Wei Tu
Washington University in St. Louis

Joong H. Kim
Washington University School of Medicine

Jian Wang
Washington University School of Medicine

Sheng-Kwei Song
Washington University School of Medicine

JOURNAL OF NEUROTRAUMA 27:253–262 (January 2010)

DOI: 10.1089/neu.2009.1026

Full Tensor Diffusion Imaging Is Not Required To Assess the White-Matter Integrity in Mouse Contusion Spinal Cord Injury

Tsang-Wei Tu,[1] Joong H. Kim,[2] Jian Wang,[2] and Sheng-Kwei Song[2]

Abstract

In vivo diffusion tensor imaging (DTI) derived indices have been demonstrated to quantify accurately white-matter injury after contusion spinal cord injury (SCI) in rodents. In general, a full diffusion tensor analysis requires the acquisition of diffusion-weighted images (DWI) along at least six independent directions of diffusion-sensitizing gradients. Thus, DTI measurements of the rodent central nervous system are time consuming. In this study, diffusion indices derived using the two-direction DWI (parallel and perpendicular to axonal tracts) were compared with those obtained using six-direction DTI in a mouse model of SCI. It was hypothesized that the mouse spinal cord ventral-lateral white-matter (VLWM) tracts, T8–T10 in this study, aligned with the main magnet axis (z) allowing the apparent diffusion coefficient parallel and perpendicular to the axis of the spine to be derived with diffusion-weighting gradients in the z and y axes of the magnet coordinate respectively. Compared with six-direction full tensor DTI, two-direction DWI provided comparable diffusion indices in mouse spinal cords. The measured extent of spared white matter after injury, estimated by anisotropy indices, using both six-direction DTI and two-direction DWI were in close agreement and correlated well with histological staining and behavioral assessment. The results suggest that the two-direction DWI derived indices may be used, with significantly reduced imaging time, to estimate accurately spared white matter in mouse SCI.

Key words: assessment tools; biomarkers; *in vivo* studies; MRI; traumatic spinal cord injury

Introduction

Spinal cord injury (SCI) results in devastating functional disabilities in patients. Due to the interference of spinal shock with the functional assessment of SCI patients in the clinical setting, it is important to develop a noninvasive imaging technique for acute evaluation of spinal cord integrity after injury. Diffusion tensor imaging (DTI) has been applied in rodent models of SCI to assess the spinal cord white-matter tract integrity (Deo et al., 2006; Ford et al., 1994; Fraidakis et al., 1998; Inglis et al., 1997; J.H. Kim et al., 2007, 2009; Loy et al., 2007; Nevo et al., 2001; Schwartz and Hackney, 2003; Schwartz et al., 2005). The extent of spared white matter may be estimated noninvasively using the DTI derived directional diffusivity, i.e., axial ($\lambda_{\|}$) and radial diffusivity ($\lambda_{\perp}$), following injury (J.H. Kim et al., 2007, 2009; Nevo et al., 2001).

Multiple directions of diffusion-weighting gradients are needed to accurately reflect white-matter structure in the human brain. The optimal number and orientations of unique gradients in estimating the diffusion tensor quantities have been extensively researched (Hasan et al., 2001; Jones, 2004; Jones et al., 1999). In general, when time is limited, at least six diffusion-weighted images (DWI) are required to derive the diffusion tensor. The white-matter structure of the spine is less complicated than that of the brain. Thus, it would be possible in the spine to choose a simpler sampling scheme, to minimize the scan time, while still obtaining adequate information to indentify white-matter structure (Clark et al., 2000; Gulani et al., 1997; Inglis et al., 1997; Schwartz and Hackney, 2003).

Several *ex-vivo* studies have characterized SCI by correlating apparent diffusion coefficient (ADC) values with the degree of injury (Ford et al., 1994; Gulani et al., 1997; Nevo et al., 2001; Schwartz et al., 2005). Ford and associates (1994) measured diffusion coefficients along the longitudinal (z) and transverse (y) axes. They found significant decreases in the longitudinal ADC value and increases in the transverse ADC

[1]Department of Mechanical, Aerospace and Structural Engineering, Washington University in St. Louis, Missouri.
[2]Department of Radiology, Washington University in St. Louis, Missouri.

value at 7 days after injury. Based on the assumption of cylindrical symmetry of the excised spinal cord, Gulani and associates (1997) showed that four of the six unique elements (D_{zz}, D_{xx}, D_{yy}, D_{xy}) in the diffusion tensor were sufficient to study the spinal cord. Nevo and associates (2001) and Schwartz and associates (2005) used two orthogonal diffusion gradient directions ($ADC_{\parallel}$ and $ADC_{\perp}$) to demonstrate that the resulting diffusion anisotropy index (AI) was a simple and scalable parameter that documented the tissue degeneration and treatment effect after injury. *Ex-vivo* samples offer the advantage of avoiding physiological noise, allowing a more controlled data acquisition. However, fixed tissues suffer from complications, including anatomic distortion resulting from fixation and significantly reduced ADC values (T.H. Kim et al., 2009; Schwartz and Hackney, 2003).

Fraidakis and associates (1998) used longitudinal (ADC_z) and transverse (ADC_x or ADC_y) diffusion gradients to assess the integrity of the rat spinal cord after injury *in vivo*. Significantly decreased longitudinal ADC_z and increased transverse ADC_x were observed. A quotient $Q_{z/x}$ ($= ADC_z/ADC_x$) was proposed as a marker, reflecting the severity of white-matter tract degeneration. Clark and associates (2000) showed that for a cylindrically symmetric spinal cord, appropriately oriented in the imaging gradient axes, it is possible to estimate the principal diffusivities and rotationally invariant measures by using a pair of diffusion-weighted scans. Gullapalli and associates (2006) reported that the principal diffusivities of diffusion tensors reflect morphologic differences between white-matter tracts that are not well appreciated with either the trace (Tr) or the fractional anisotropy (FA). However, to the best of our knowledge, no studies to date have systematically compared measurements between simplified gradient-encoding schemes, such as two- or four-direction DWI, and the full tensor DTI scheme with appropriate validation using the "gold-standard" histology.

In the present study, the two-direction DWI and six-direction DTI measurements were employed to evaluate the extent of spared white matter in mice after SCI. Results were correlated with histologicallly determined spared white matter (Laxol Fast Blue, LFB) and open field tests of hindlimb locomotor function, evaluated using the Basso Mouse Scale (BMS) (Basso et al., 2006).

Methods

Spinal cord injury

All surgical preparations and pre- and postsurgical care were provided in accordance with Public Health Service Policy on Humane Care and Use of Laboratory Animals and Guide for the Care and Use of Laboratory Animals (Institute of Laboratory Animal Resources, National Research Council, 1996), and with the approval of the Washington University Animal Studies Committee.

Twelve 10–12-week-old female C57BL/6 mice, weighing 18–22 g (Harlan Sprague Dawley, Inc., IN), were anesthetized with an isoflurane/oxygen mixture. Seven mice received mild contusion SCI utilizing a modified Ohio State University (OSU) impactor after dorsal laminectomy at the T9 vertebral level. The remaining five mice underwent a laminectomy without contusion and served as the control. The surgical site was closed in layers with 4-0 vicryl and nylon sutures. Injections of enrofloxacin (2.5 mg/kg) and lactated ringers (1.5 ml) were given subcutaneously. Manual bladder expression in injured mice was performed twice daily throughout the duration of the study (Jakeman et al., 2000). Softened rodent chow was provided. Body weights were measured and compared daily with the preoperative weight. High-calorie nutrient paste (Nutrical; Evsco, Inc., Buena, NJ) was given to the mice to maintain body weights at 90% of their preoperative values. All mice that received impact injuries exhibited partial paralysis with some spontaneous hindlimb movements. In contrast, the sham-operated animals exhibited essentially normal overground locomotion. All injured mice were evaluated by BMS scores daily for 1 to 14 days after injury.

Animal preparation for in vivo *diffusion MRI*

Mice were anesthetized with an isoflurane/oxygen mixture (4.5–5% isoflurane for induction and 0.7–1.5% isoflurane for maintenance). Core body temperatures were maintained at 37°C with a circulating warm-water pad. The inhalant anesthetic was delivered to the mice through a custom-made nose cone. The respiratory exhaust line was connected to a pressure transducer to synchronize DTI data collection with the animal's respiratory rate (J.H. Kim et al., 2006).

An MRI-compatible device was utilized to stabilize the vertebral column as reported previously (J.H. Kim et al., 2006). An inductively coupled surface receiver coil covering vertebral segments T6–T12 (15 mm×8 mm) was used as the receiver. A 9-cm (inner diameter) Helmholtz coil was employed as the RF transmitter. The alignment of spine segments to the magnet *z*-axis was carefully adjusted and confirmed by scout images. The entire preparation was placed in a 4.7 T magnet (Oxford Instruments plc, Abingdon, UK) equipped with a 15-cm (inner diameter) actively shielded Magnex gradient coil (60 G/cm, 270 μs rise time). The magnet, gradient coil, and IEC gradient power supply were interfaced with a Varian DirectDrive console (Varian, Inc., Palo Alto, CA).

In vivo *diffusion tensor imaging*

In vivo diffusion measurements were conducted at 14 days after injury for comparing injury severities among animals after stable functional recovery was reached. A spin-echo sequence, modified by adding Stejskal–Tanner diffusion-weighting gradient (Stejskal and Tanner, 1965), was used. Diffusion-weighted images for both six- and two-direction diffusion measurements were performed in an interleaved fashion. The following parameters were used for all measurements: spin-echo time (TE) = 38 ms, time between the application of gradient pulses (Δ) = 21 ms, diffusion gradient on time (δ) = 7 ms, diffusion-gradient amplitude = 12.5 G/cm, number of averages = 8, field of view (FOV) = 1×1 cm, and data matrix = 128×128 (zero-filled to 256×256). The repetition time (TR ≈ 1.2 s) was varied according to the period of the respiratory cycle (~270 ms). A single line of k-space from each of three different image slices was collected with every breath. Two diffusion-sensitizing *b* values of 0 and 1.02 ms/μm^2 were used. Nine transverse images (slice thickness = 0.75 mm) were collected covering vertebral segments T8–T10.

Six diffusion-sensitizing gradients were employed, corresponding to the 12 cube edges, for DTI analysis: $(G_x,G_y,G_z) = (1,1,0), (1,0,1), (0,1,1), (-1,1,0), (0,-1,1), (1,0,-1)$. Three eigenvalues ($\lambda_1$, λ_2, λ_3) were calculated from the diffusion tensor matrix. Mean diffusivity ($\langle D \rangle$) was calculated by

$\langle D\rangle = (\lambda_1 + \lambda_2 + \lambda_3)/3$. Axial diffusivity was defined as $\lambda_{\|} = \lambda_1$. Radial diffusivity was defined as $\lambda_{\perp} = (\lambda_2 + \lambda_3)/2$. The scaled relative anisotropy (Asd) was calculated as:

$$Asd = \frac{\sqrt{(\lambda_1 - <D>)^2 + (\lambda_2 - <D>)^2 + (\lambda_3 - <D>)^2}}{\sqrt{2}(\sqrt{3}<D>)} \quad (1)$$

Asd ranges from 0 to 1, for direct comparison with the anisotropy index (AI), were derived using the six-direction scheme (Armitage and Bastin, 2000).

Two diffusion-sensitizing gradients were employed for the two-direction DWI: $(G_x, G_y, G_z) = (1,1,0)$, and $(0,0,1)$. Apparent diffusion coefficient parallel ($D_{\perp}$) and perpendicular ($D_{\perp}$) to axonal tracts as well as the AI were directly obtained from the relationship of signal intensity $[S_n(b)]$ to the b value given by equations (2) and (3) (independent of tensor analysis).

$$S_n(b) = S_0 \cdot e^{-b \cdot D} \quad (2)$$

$$D = \frac{\ln[S_0(b)/S_n(b)]}{b} \quad (3)$$

The AI was derived according to Eq. (4):

$$AI = \frac{D_{\|} - D_{\perp}}{D_{\|} + D_{\perp}} \quad (4)$$

All parameters were derived from diffusion-weighted images using software written in Matlab (MathWorks, Natick, MA). Three slices were averaged to obtain the value of each vertebral segment. The acquisition time was approximately 3.0 h for the six-direction DTI and 1.3 h for the two-direction DWI.

Region of interest analyses

The boundary between ventral-lateral white matter (VLWM) and ventral gray matter (GM) was identified on Asd and AI maps. Regions of interest (ROIs) encompassing the total white matter were manually delineated for VLWM (control and injured cords) and GM (control cords only) on anisotropy maps. The anisotropy distributions of both GM and VLWM were obtained from five sham-operated control animals for a histogram analysis of Asd and AI respectively. The mean and standard deviation (SD) were determined and a threshold (mean $\pm$ 2$\times$SD) was used to define the spared VLWM in contusion injured cords on both Asd and AI maps (designated by ROI_{Asd} and ROI_{AI}; Fig. 1). Spared VLWMs of injured cords were then normalized to the total VLWMs of control cords to remove the atrophic effect of the injured cord for the comparison with the gold-standard histology defined spared VLWM extent.

Overlap index of regions of interest

To show that two- and six-direction diffusion measurements were detecting the same region of spared VLWM, an overlap index comparing ROI_{Asd} and ROI_{AI} was calculated to quantify the degree of overlap by:

$$\underset{Index}{Overlap} = \frac{[(ROI_{Asd} \cap ROI_{AI})/ROI_{Asd}] + [(ROI_{Asd} \cap ROI_{AI})/ROI_{AI}]}{2} \quad (5)$$

where $ROI_{Asd} \cap ROI_{AI}$ are the overlapping pixels. The formula estimates the mean overlap index for the partitions in ROI_{Asd} and ROI_{AI}. Kung and associates (2007) performed a Monte Carlo simulation, suggesting that this formula is less

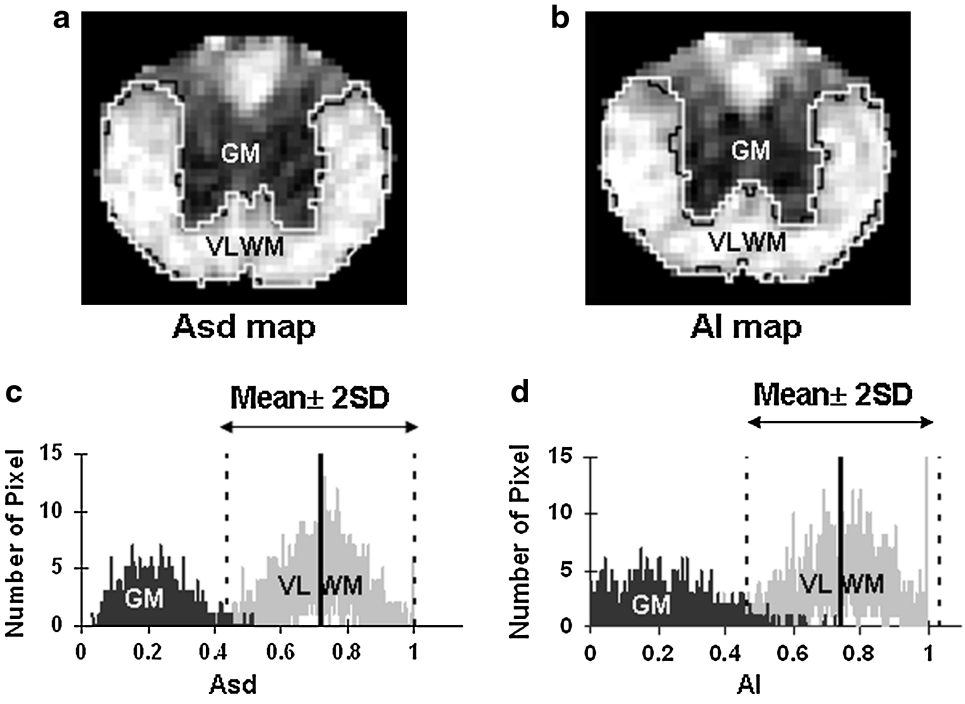

FIG. 1. The manual (black) and threshold (white) segmentation of normal-appearing VLWM in Asd (**a**) and AI (**b**) maps of a control cord. Two normal distributions of the pixel numbers of anisotropy were observed in manually defined GM and VLWM in Asd (**c**) and AI (**d**) map. The mean $\pm$ 2$\times$SD (95.4% confidence interval) of VLWM was used as the threshold to define the region of normal-appearing VLWM in the control and injured spinal cords, designated as ROI_{Asd} and ROI_{AI}.

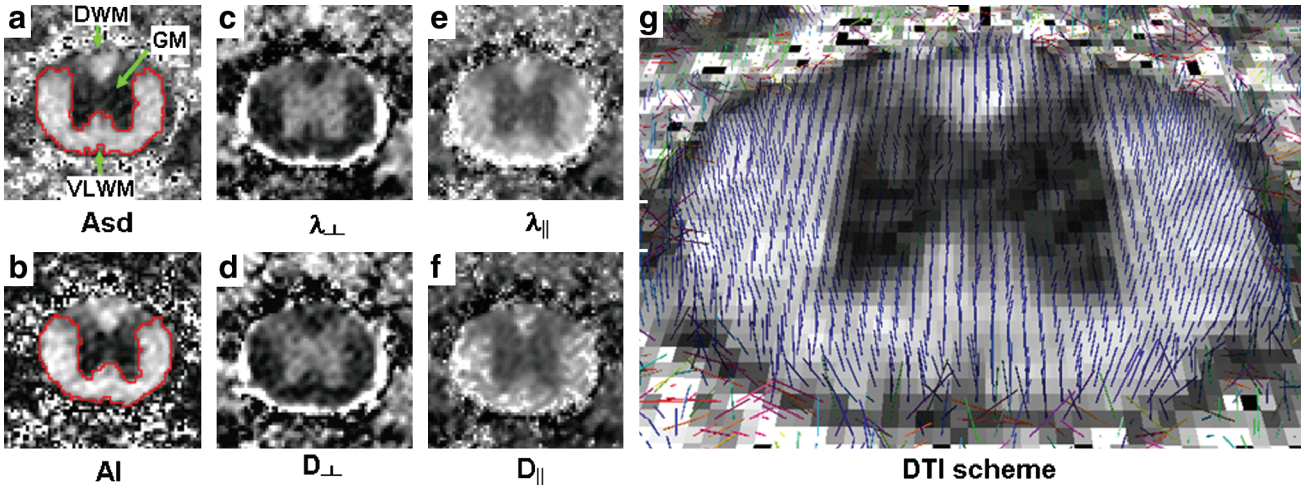

FIG. 2. Representative control spinal cord images of T9 vertebra level obtained from DTI and DWI: diffusion anisotropy, Asd, and AI (**a, b**); diffusivity transverse to the white-matter tract, $\lambda_\perp$ and $D_\parallel$ (**c, d**); and diffusivity parallel to the fiber tract, $\lambda_\perp$ and $D_\perp$. (**e, f**). Cerebral spinal fluid (CSF) is clearly seen in the $\lambda_\perp$, $D_\perp$, $\lambda_\parallel$ and $D_\parallel$ maps, enabling the identification of the cord parenchyma. Regions of dorsal white matter (DWM), ventral-lateral white matter (VLWM), and gray matter (GM) are readily visualized in the anisotropy maps, as well as in all other diffusion index maps. The manually segmented ROI of GM and VLWM were used to quantify the group-averaged parameters of each region. The pixel-based whisker plots show the principal diffusion direction obtained by DTI scheme (**g**, with Asd background) based on the calculation of tensor eigenvectors in each pixel. Color image is available online at www.liebertonline.com/neu.

sensitive to the variation of ROI sizes (i.e., best suited for comparing different-sized ROIs). The index ranges from 0% (completely mismatching) to 100% (completely overlapping).

Behavioral assessment of hindlimb locomotor function

Animals were scored using BMS over the 14-day recovery period (Basso et al., 2006). The test is taken by two or more evaluators with a scoring system from 1 (worst) to 9 (best), plus a subscore tally from 0 (worst) to 11 (best). Mouse hindlimb locomotor function is scored by angle movement, plantar placement, stepping, coordination, paw position, trunk instability, and tail position. In this study, the mild contusion SCIs resulted in BMS scores ranging from 6 to 9 on the injured mice and 9 on the laminectomy controls at 14 days after injury.

Tissue preparation and histological analysis

Immediately after imaging, mice were perfusion fixed under deep anesthesia with 50 mL of 0.1 M phosphate-buffered saline (PBS) (pH 7.4) followed by 200 mL of 0.1 M PBS containing 4% paraformaldehyde (pH 7.4). Following fixation, the spine was excised, left in the fixative overnight, decalcified for 48 h, embedded in paraffin, and sectioned on a sliding microtome (5 μm) with the decalcified vertebral column intact. For the examination of the extent of spared VLWM, LFB (Sigma, Saint Louis, MO) staining was conducted. After deparaffinization, rehydration, and immersion in 1% LFB in 95% ethanol and 0.5% acetic acid, the excess stain was rinsed off and differentiated using 0.05% $LiCO_3$ solution (56°C). Tissue was then mounted for microscopic inspection after completion of differentiation.

Stained sections at the injury epicenter were digitally imaged using a Nikon Eclipse 80i microscope (Nikon Corporation, Tokyo, Japan) equipped with a 4× objective, and the images were captured with a Photometrics CCD digital camera using MetaMorph image acquisition software (Universal Imaging Corporation, Downington, PA). All images were captured within 1 week following completion of histological staining. The area of positive staining was quantified by the pixel grayscale value threshold of 95.4% of the intensity from the intact nerve root. The spared VLWM area was then normalized to the total VLWM area. All images were calculated using NIH ImageJ v1.37 (Rasband, 1997–2005). All slides were assessed blindly with respect to the injury.

Statistical analysis

Statistical analysis was performed with SAS (V9.1.3, SAS Institute, Inc., Cary, NC). Data were expressed as mean and standard deviation (SD). A paired Student's *t*-test was performed comparing two- and six-direction diffusion measurements with $p < 0.05$ regarded as statistically significant. Correlations between normalized normal-appearing VLWM areas determined by AI, and Asd were examined with Pearson correlation using seven injured animals, each with nine slices. The images correlated with LFB and BMS were obtained from one slice at the injury epicenter. The correlation coefficient (r) with the p-value is reported.

Results

Diffusion index maps, acquired from both DTI and DWI at 14 days after injury, provide similar tissue contrast in the control cords (Fig. 2). White matter appeared bright in both Asd and AI maps. The less anisotropic gray matter appeared dark. In both maps, the distinct border between gray and white matter enabled manual segmentation of dorsal white matter (DWM), GM, and VLWM. Furthermore, the cerebrospinal fluid (CSF) was hyperintense in both $\lambda_\perp$ and $D_\perp$ maps,

Table 1. Group-Averaged Diffusion Parameters at T9 in the Control Spinal Cords

	Segment	*Asd*	*AI*	p	$\lambda_\perp$ ($\mu m^2/ms$)	$D_\perp$ ($\mu m^2/ms$)	p	$\lambda_\parallel$ ($\mu m^2/ms$)	$D_\parallel$ ($\mu m^2/ms$)	p
VLWM	T8	0.70 ± 0.02	0.73 ± 0.04	< 0.05	0.28 ± 0.03	0.29 ± 0.04	0.59	2.07 ± 0.10	1.84 ± 0.14	<0.01
	T9	0.71 ± 0.02	0.75 ± 0.03	< 0.05	0.26 ± 0.02	0.26 ± 0.03	0.45	2.01 ± 0.07	1.80 ± 0.11	<0.01
	T10	0.71 ± 0.02	0.74 ± 0.02	<0.05	0.24 ± 0.03	0.25 ± 0.03	0.19	1.93 ± 0.09	1.73 ± 0.08	<0.01
GM	T8	0.26 ± 0.04	0.26 ± 0.04	0.99	0.55 ± 0.06	0.57 ± 0.04	0.29	1.07 ± 0.08	0.98 ± 0.08	<0.05
	T9	0.22 ± 0.03	0.24 ± 0.05	0.37	0.59 ± 0.04	0.59 ± 0.04	0.97	1.03 ± 0.07	0.96 ± 0.08	<0.05
	T10	0.21 ± 0.03	0.17 ± 0.03	<0.05	0.58 ± 0.04	0.60 ± 0.04	0.14	0.95 ± 0.05	0.85 ± 0.04	<0.01
VLWM/GM	T8	2.75 ± 0.36	2.84 ± 0.31	0.45	0.45 ± 0.11	0.50 ± 0.05	0.16	1.94 ± 0.10	1.88 ± 0.13	0.16
	T9	3.28 ± 0.42	3.27 ± 0.59	0.96	0.39 ± 0.09	0.45 ± 0.05	0.06	1.95 ± 0.09	1.87 ± 0.11	0.07
	T10	3.56 ± 0.54	4.55 ± 0.68	<0.01	0.39 ± 0.10	0.42 ± 0.04	0.89	2.04 ± 0.06	2.04 ± 0.06	0.27

The data were obtained from the manually segmented VLWM and GM.

Diffusion indices were derived using DTI and DWI data from the control cords of the manually defined VLWM and gray matter ROIs. Values (mean $\pm$ SD) were obtained from all three slices of each vertebral segment. Statistical analysis was performed using a two-tailed, paired Student's *t*-test with a confidence interval of 95%. The *p* value indicates the level of statistical difference between diffusion indices obtained from six-direction DTI and two-direction DWI.

facilitating segmentation of the parenchyma of the cord. Unlike the more complete diffusion information provided in the full tensor image, the two-direction DWI scheme only measured the diffusion perpendicular and parallel to the spinal cord tract. The alignment of the spinal cord to the magnet *z*-axis was reaffirmed by the consistency between the directions of principal diffusion in DTI (Fig. 2g) and the magnet *z*-axis.

The group-averaged diffusion parameters of the manually segmented VLWM and GM in the control spinal cord are listed in Table 1. Consistent with our previous reports, $\lambda_\parallel$ was higher in VLWM than in GM, and $\lambda_\perp$ was higher in GM than that in VLWM (J.H. Kim et al., 2006, 2007; Loy et al., 2007). The same trend was also seen in $D_\perp$ and $D_\perp$. Overall, $\lambda_\parallel$ and $D_\parallel$ were approximately seven-fold the values of $\lambda_\perp$ and $D_\perp$ in VLWM, and two-fold those in GM. $D_\parallel$ was slightly lower than

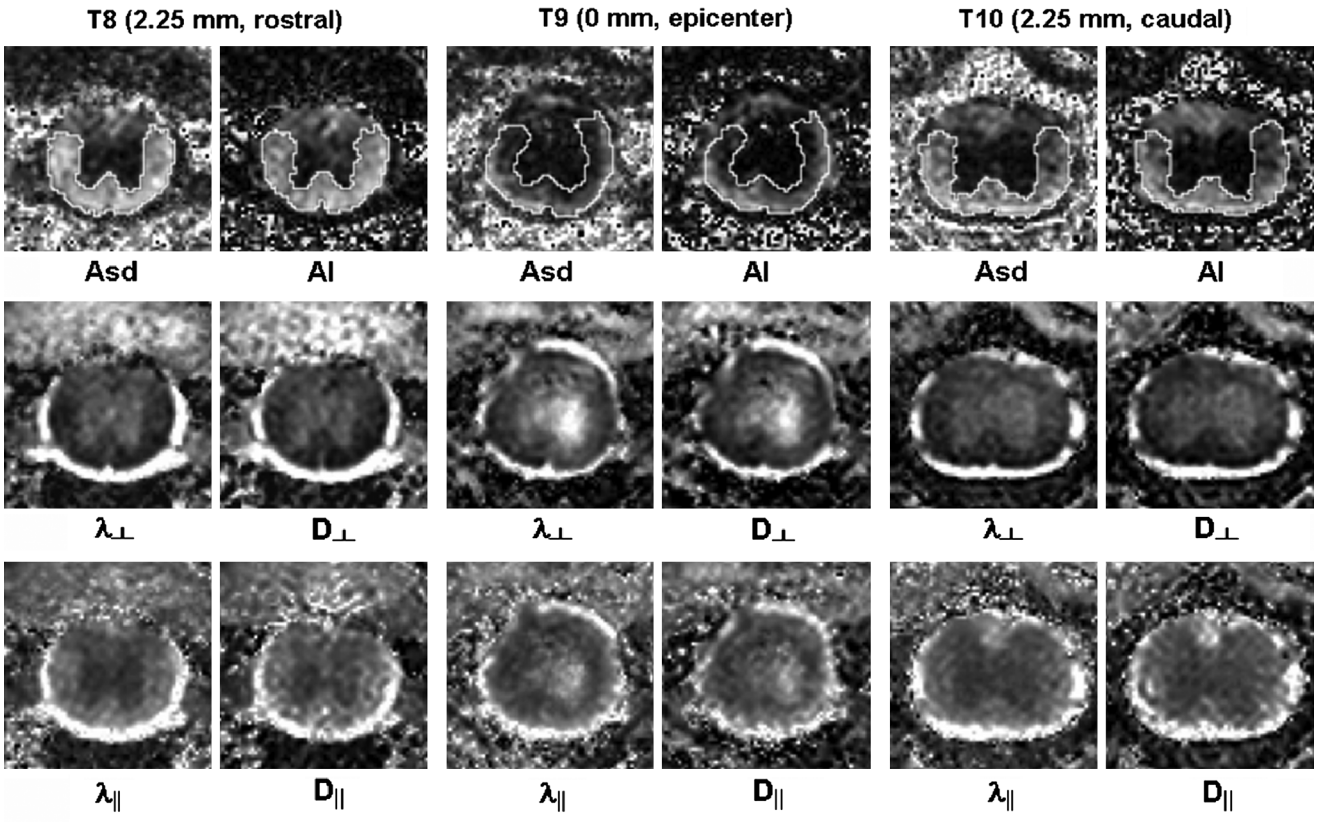

FIG. 3. Representative images of the injured spinal cord from DTI (left column in each panel) and DWI (right column in each panel) covering segments of T8 (2.25 mm rostral), T9 (0 mm, epicenter), and T10 (2.25 mm caudal) are presented. Both schemes provide good-quality images of the injured cords, enabling easy ROI analysis. The manually segmented ROIs of total VLWM on the anisotropy maps at T8, T9 (epicenter), and T10 were used to quantify the group-averaged value of each slice (data shown in Fig. 4). In the Asd and AI maps, the residual normal-appearing VLWM represents the spared white matter where the myelinated axons are mostly intact.

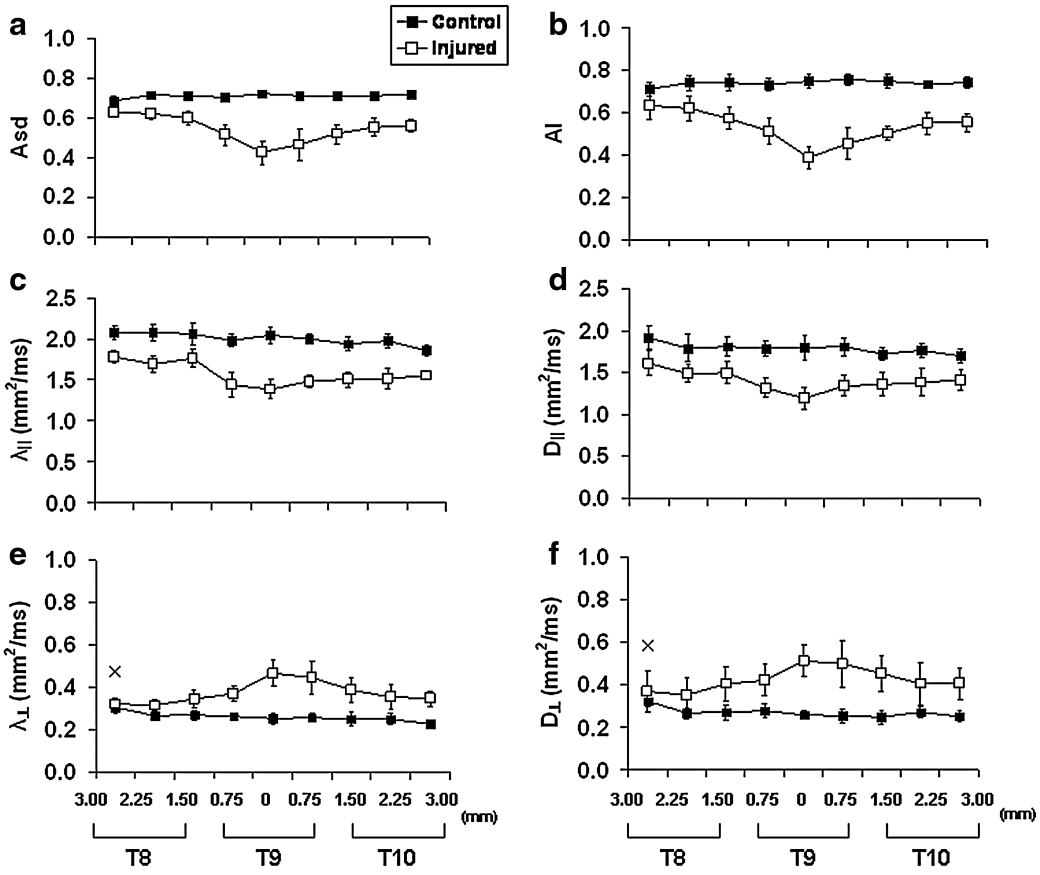

FIG. 4. Spatial evolutions of DTI (**a, c, e**) and DWI (**b, d, f**) parameters from T8 to T10 in the control (■) and injured (□) cords. Decreased $\lambda_{||}$ and $D_{||}$ (c, d), and increased $\lambda_{\perp}$ and $D_{\perp}$ (e, f) are seen at the injury epicenter. At 14 days following the contusion SCI, both DTI and DWI measured the same trend of changing diffusion indices, reflecting both axon and myelin damages at the site of impact. Group-averaged Asd and AI of a contusion injured spinal cord clearly demonstrate the spatial evolution of the injury. The quantification was done by manually defined ROIs of total VLWM. All parameters between the control and injured groups are statistically significantly different at all image slices except the first slice, marked with ×, of $\lambda_{\perp}$ and $D_{\perp}$.

$\lambda_{||}$ in both GM and VLWM ($\sim$10%, $p < 0.01$), while $D_{\perp}$ and $\lambda_{\perp}$ had no significant difference. AI was slightly higher than Asd in VLWM ($\sim$3%, $p < 0.05$). However, there was no difference between AI and Asd in GM except in the T10 vertebral segment ($\sim$10%, $p < 0.05$).

In the injured cord, the contrast between VLWM and GM was reduced in the diffusion index maps of both schemes (Fig. 3). The evolution of diffusion parameters from T8 to T10 was monitored by manual ROI analysis. The trends of AI, $D_{||}$, and $D_{\perp}$ paralleled that of Asd, $\lambda_{||}$, and $\lambda_{\perp}$ (Fig. 4). Both DTI and DWI detected a similar trend of decreased diffusion anisotropy, decreased axial diffusivities, and increased radial diffusivities in the VLWM tract, indicating axonal injury and myelin damage.

After applying thresholds to the Asd (0.42) and AI (0.48) maps, the regions of normal-appearing VLWM were compared and evaluated by the overlap index (Fig. 5a). An agreement of $>$93% in Asd- and AI-detected normal-appearing VLWM was evident, with a significant ROI overlap. The difference between ROI_{Asd} and ROI_{AI} existed mainly at the border of VLWM, where partial volume effect is inevitable transitioning between tissue types (Fig. 5b). The similar agreement was also seen in the normal-appearing VLWM of the injured cords. However, the degrees of overlap at the injury epicenter (75.9 $\pm$ 5.4 %) were relatively lower than that at sites 0.75 mm rostral (85.7 $\pm$ 2.2 %) or caudal (83.2 $\pm$ 3.0 %) to the epicenter. The degrees of overlap of control cords showed no difference among all segments. The normalized area measured using Asd or AI from T8 to T10 was comparable (Fig. 6a and 6b).

The spinal cords were stained with LFB to assess the contents of spared VLWM from the epicenter at 14 days after injury. Myelinated tracts of the dorsal, ventral, and lateral white matter were stained blue in normal controls (Fig. 7a). After the contusion SCI, the injury resulted in extensive loss of LFB stained area in the white matter (control: $0.98 \pm 0.04\,mm^2$; injury: $0.61 \pm 0.15\,mm^2$). The MR-determined normal-appearing VLWM and LFB-determined spared VLWM were in close agreement (Fig. 7b). Furthermore, the spared VLWM areas also correlated with BMS (Fig. 7c).

Discussion

In this study, the capability of detecting mouse spinal cord VLWM injury using six-direction DTI and two-direction DWI was compared. Our results showed comparable image qualities from both schemes, allowing segmentations of the region of DWM, GM, and VLWM. Fourteen days after injury, both $\lambda_{||}$

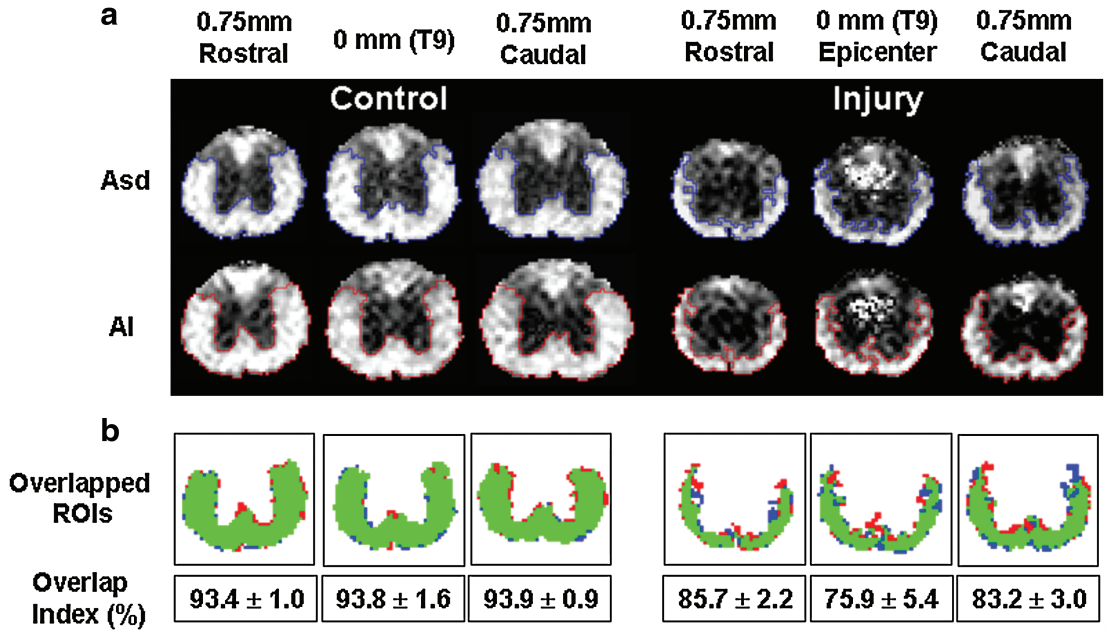

FIG. 5. (**a**) Normal-appearing VLWM of control (left panel) and injured cords (right panel) were estimated using Asd and AI thresholds. Three representative images from each cord (epicenter, i.e., 0 mm, and 0.75 mm rostral and caudal to the epicenter) at T9 vertebra level were compared. (**b**) The pixels identified within both ROI_{Asd} and ROI_{AI} are color coded in green. The inconsistent pixels are marked in red (outside of ROI_{Asd}) and blue (outside of ROI_{AI}). The major discrepancy is seen at the border of gray–white matter and parenchyma–CSF. In general, the overlap index averaged ~94% for the control cords ($n=5$), and ~80% for that of injured cords ($n=7$). Color image is available online at www.liebertonline.com/neu.

and $D_{\parallel}$ decreased, while both $\lambda_{\perp}$ and $D_{\perp}$ increased, suggestive of axonal and myelin damage respectively. Significant overlap of Asd- and AI-determined normal-appearing VLWM was observed: ~93% for the control cords and ~80% for mild-to-moderately injured cords. The detected spared VLWM were validated by LFB staining and correlated with the BMS scores. The acquisition time for the two-direction DWI was 57%; shorter than the time required for the six-direction DTI.

The role of DTI parameters in evaluating the contusion SCI white-matter pathology was recently investigated (Deo et al., 2006; Ford et al., 1994; Fraidakis et al., 1998; J.H. Kim et al., 2007, 2009; Loy et al., 2007; Nevo et al., 2001). The decreased $\lambda_{\parallel}$ correlated with axonal injury, while the increased $\lambda_{\perp}$ reflected myelin damage. Loy and associates (2007) further demonstrated that $\lambda_{\parallel}$ is able to differentiate the injury severity in the hyperacute phase (within 6 h of injury). Our other reported studies also demonstrated that increased $\lambda_{\perp}$ paralleled the myelin damage secondary to retinal ischemia in the mouse optic nerve (Song et al., 2003; Sun et al., 2008). The diffusion anisotropy reflects the combined effect of $\lambda_{\parallel}$ and $\lambda_{\perp}$, and is capable of detecting white-matter integrity (without distinguishing axonal vs. myelin damage) (J.H. Kim et al., 2007, 2009). Similarly, the measured $D_{\parallel}$ and $D_{\perp}$, from the two-direction DWI, also reflected the axonal and myelin injury in the present study (Fig. 4). Although statistically significant differences were seen between $\lambda_{\parallel}$ and $D_{\parallel}$ (~10%) as well as Asd and AI (~3%) in the control animals, the two-direction DWI indices correctly reflected the injury extent in the SCI animals as assessed by DTI. At 14 days after injury, our data showed the decreased $\lambda_{\parallel}$ and $D_{\parallel}$ and the increased $\lambda_{\perp}$ and $D_{\perp}$ in the SCI animals without a significant difference between

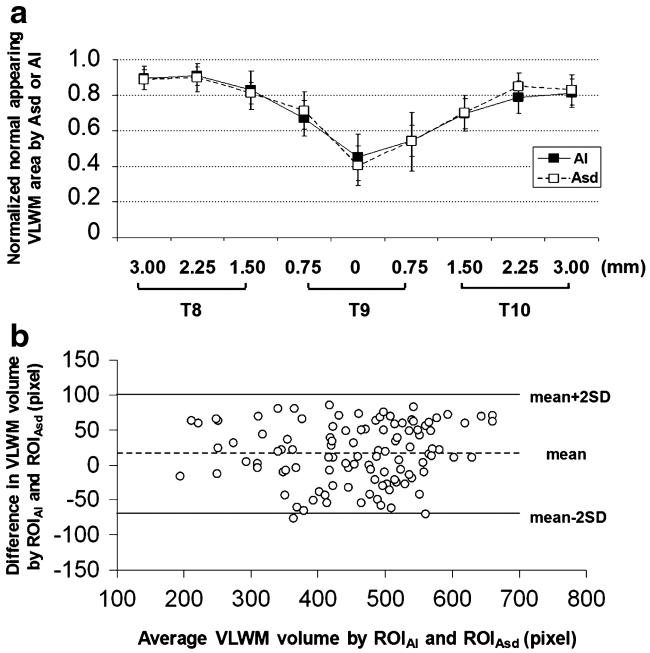

FIG. 6. (**a**) The normal-appearing VLWM areas of the injured cords were assessed using Asd and AI. The areas were normalized by the amount of total VLWM of the control cords ($r=+0.89$, $n=63$, $p<0.0001$). (**b**) A Bland–Altman plot displays the difference of normal-appearing VLWM areas determined by Asd and AI against the average of Asd and AI assessments from the 108 paired measurements in the study. The difference between normal-appearing VLWM measurements using Asd and AI lies within the limit of agreement (95%, mean ± 2×SD).

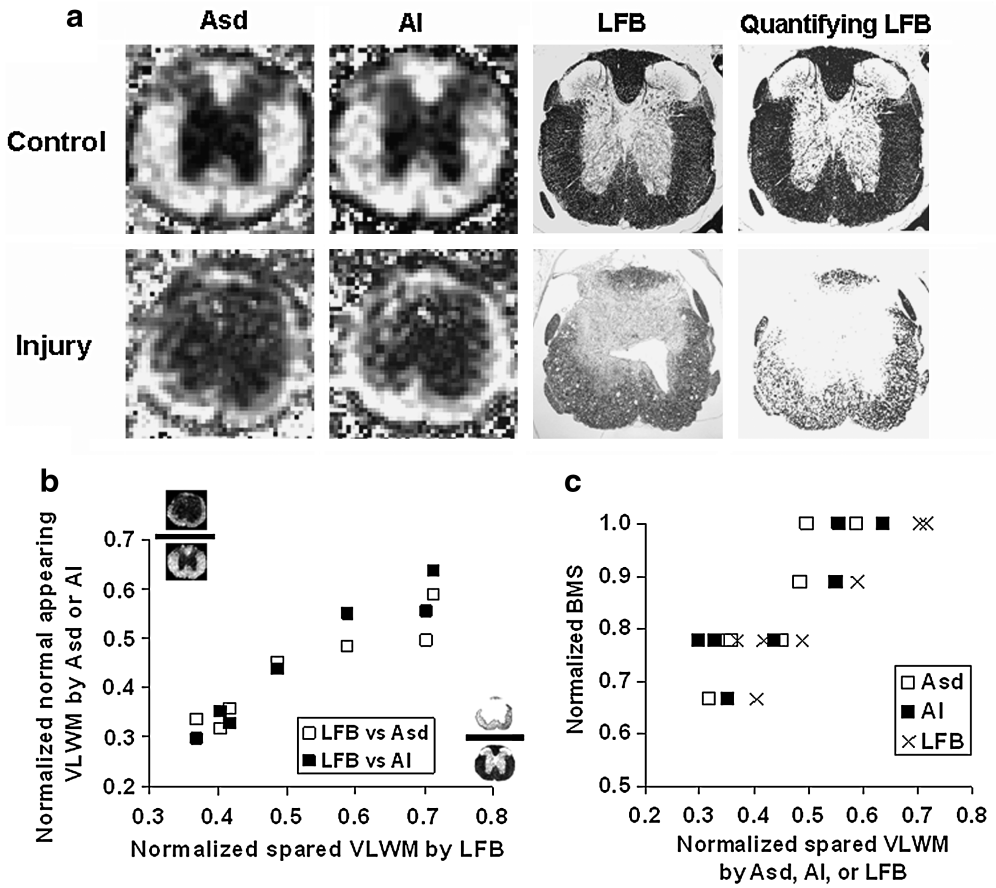

FIG. 7. (**a**) Corresponding images of Asd, AI, and LFB staining. The gray-scaled LFB images are normalized by the LFB staining intensity of the uninjured nerve roots to quantify the extent of spared VLWM. In the control cords, images from DTI, DWI, and histological staining show a similar pattern across the region of VLWM, indicating the integrity of axons and myelin sheaths. For the injured cords, mild to moderate white-matter injuries were observed in the histological maps at the impact epicenter at 14 days after injury, consistent with the Asd and AI maps. (**b**) The correlation between the normalized LFB and Asd/AI assessed normal-appearing VLWM. (LFB vs. Asd: $r = +0.97$, $n = 7$, p (correl) < 0.001; LFB vs. AI: $r = +0.95$, $n = 7$, p (correl) $= 0.001$). (**c**) Spared VLWM areas assessed using all three methods correlated well with the BMS scores at 14 days after injury. (LFB vs. BMS: $r = +0.86$, $n = 7$, p (correl) $= 0.01$; Asd vs. BMS: $r = +0.89$, $n = 7$, p (correl) < 0.01; AI vs. BMS: $r = +0.87$, $n = 7$, p (correl) $= 0.01$).

the two schemes of measurements. The difference between the $\lambda_{\|}$ and $D_{\|}$ in the control animals might be caused primarily by the inherently different signal attenuations between different diffusion encoding schemes (i.e., six-direction 12-cube-edge and two-direction orthogonal encoding). The data from the injured cord group still demonstrated the adequacy of two-direction DWI in detecting axonal and myelin damages.

The efficacy of therapeutic interventions on the functional recovery of rodent SCI has been evaluated by examining the extent of spared white matter (Basso et al., 1996; Casha et al., 2005; Farooque et al., 2001). In a series of rat studies, Basso (2000) analyzed locomotor outcomes after mild, moderate, or severe spinal cord contusion with extensive (>40%), intermediate (15–40%), or minimal (1–14%) tissue sparing determined by LFB staining at the lesion epicenter. They found that locomotor recovery was extensive after mild SCI with extensive axonal sparing (>40%), but was quite limited after severe SCI with little sparing (as low as 1–2%). Our recent study investigating the effect of different impact speeds ranging from 0.1 to 0.4 m/s on the severity of contusion SCI (J.H. Kim, 2009) demonstrated that *in vivo* DTI-estimated spared VLWM content in the subacute phase correlated well with those determined using postmortem histology and behavioral test in the chronic phase.

In the present study, all the injured mice showed intermediate to extensive recovery, with 30–60% preserved normal-appearing VLWM. Although LFB staining consistently estimated larger preserved VLWM areas than MR measurements, probably due to the residual myelin debris, the correlation between histology and MR images was statistically significant. Most importantly, the MR-estimated extent of spared white matter correlated with behavioral scores (Fig. 7c). These findings support that tissue sparing at the lesion epicenter determined in the subacute phase (7–14 days after injury) correlates with the chronic behavioral disability (14–21 days after injury) in the experimental spinal cord contusion.

Early studies using a two-direction DWI scheme to study the spinal cord have been performed by accurately aligning

the cord to the magnet axes. This was easily achieved on *ex-vivo* tissues. However, for an *in vivo* study, it is more difficult to align the spinal cord to the magnet axes of reference. If the segment of interest fails to align with an axis in the magnet frame of reference while the diffusion-weighting gradient is still aligning with the magnet axes, the measured ADC values need to be corrected (Clark et al., 2000). In the current study, we attempted to reproduce the findings in the literature, with the spine and diffusion-weighting gradients aligning with the magnet axes. The correct cord alignment was confirmed by the fact that the principal eigenvector of the white-matter tract (Fig. 2g,h) derived from the diffusion tensor imaging were parallel to the magnet *z*-axis. However, when imaging of the entire human spinal cord is attempted, the curvature of the spine would make it difficult to align the axis of the spine with the magnet *z*-axis. To employ the two-direction DWI for ADC measurements in this instance, parallel and perpendicular diffusion-weighting gradients would need to be aligned according to the curvature of different segments. As the gradients can be manipulated arbitrarily nowadays, small segments of spine could be imaged in this fashion by first assessing directionality with scout images and then applying appropriate orthogonal gradients. The only drawback of using two-direction DWI would be the need to group the spinal segments according to the curvature of the SCI patients during the planning of scout images. However, this will not prohibit its use, since segmented imaging of a human spine is typically necessary even for the DTI data acquisition.

Conclusion

In conclusion, we have proven that when the animal is correctly installed, two-directional DWI could provide similar diffusion measurements as full tensor DTI to detect the spared while matter content *in vivo* in the contusion SCI.

Acknowledgments

We thank Dr. Matthew Budde for his valuable advice on the data analysis, and Hsiao-Fang Liang for her assistance on immunohistological staining. We also thank Jeff Anderson for the helpful discussion and suggestion on the manuscript. This study was supported in part by National Institute of Health NS047592 and the University of Missouri Spinal Cord Injuries Research Program.

Author Disclosure Statement

No competing financial interests exist.

References

Armitage, P.A., and Bastin, M.E. (2000). Selecting an appropriate anisotropy index for displaying diffusion tensor imaging data with improved contrast and sensitivity. Magn. Reson. Med. 44, 117–121.

Basso, D.M. (2000). Neuroanatomical substrates of functional recovery after experimental spinal cord injury: Implications of basic science research for human spinal cord injury. Phys. Ther. 80, 808–817.

Basso, D.M., Beattie, M.S., and Bresnahan, J.C. (1996). Graded histological and locomotor outcomes after spinal cord contusion using the NYU weight-drop device versus transection. Exp. Neurol. 139, 244–256.

Basso, D.M., Fisher, L.C., Anderson, A.J., Jakeman, L.B., McTigue, D.M., and Popovich, P.G. (2006). Basso Mouse Scale for locomotion detects differences in recovery after spinal cord injury in five common mouse strains. J. Neurotrauma 2, 635–659.

Casha, S., Yu, W.R., and Fehlings, M.G. (2005). FAS deficiency reduces apoptosis, spares axons and improves function after spinal cord injury. Exp. Neurol. 196, 390–400.

Clark, C.A., Werring, D.J., and Miller, D.H. (2000). Diffusion imaging of the spinal cord in vivo: Estimation of the principal diffusivities and application to multiple sclerosis. Magn. Reson. Med. 43, 133–138.

Deo, A.A., Grill, R.J., Hasan, K.M., and Narayana, P.A. (2006). In vivo serial diffusion tensor imaging of experimental spinal cord injury. J. Neurosci. Res. 83, 801–810.

Farooque, M., Isaksson, J. and Olsson, Y. (2001). White matter preservation after spinal cord injury in ICAM-1/P-selectin-deficient mice. Acta Neuropathol. 102, 132–140.

Ford, J.C., Hackney, D.B., Alsop, D.C., Jara, H., Joseph, P.M., Hand, C.M., and Black, P. (1994). MRI characterization of diffusion coefficients in a rat spinal cord injury model. Magn. Reson. Med. 31, 488–494.

Fraidakis, M., Klason, T., Cheng, H., Olson, L., and Spenger, C. (1998). High-resolution MRI of intact and transected rat spinal cord. Exp. Neurol. 153, 299–312.

Gulani, V., Iwamoto, G.A., Jiang, H., Shimony, J.S., Webb, A.G., and Lauterbur, P.C. (1997). A multiple echo pulse sequence for diffusion tensor imaging and its application in excised rat spinal cords. Magn. Reson. Med. 38, 868–873.

Gullapalli, J., Krejza, J., and Schwartz, E.D. (2006). In vivo DTI evaluation of white matter tracts in rat spinal cord. J. Magn. Reson. Imaging 24, 231–234.

Hasan, K.M., Parker, D.L., and Alexander, A.L. (2001). Comparison of gradient encoding schemes for diffusion-tensor MRI. J. Magn. Reson. Imaging 13, 769–780.

Inglis, B.A., Yang, L., Wirth, E.D., 3rd, Plant, D., and Mareci, T.H. (1997). Diffusion anisotropy in excised normal rat spinal cord measured by NMR microscopy. Magn. Reson. Imaging 15, 441–450.

Jakeman, L.B., Guan, Z., Wei, P., Ponnappan, R., Dzwonczyk, R., Popovich, P.G., and Stokes, B.T. (2000). Traumatic spinal cord injury produced by controlled contusion in mouse. J. Neurotrauma 17, 299–319.

Jones, D.K. (2004). The effect of gradient sampling schemes on measures derived from diffusion tensor MRI: A Monte Carlo study. Magn. Reson. Med. 51, 807–815.

Jones, D.K., Horsfield, M.A., and Simmons, A. (1999). Optimal strategies for measuring diffusion in anisotropic systems by magnetic resonance imaging. Magn. Reson. Med. 42, 515–525.

Kim, J.H., Budde, M.D., Liang, H.F., Klein, R.S., Russell, J.H., Cross, A.H., and Song, S.K. (2006). Detecting axon damage in spinal cord from a mouse model of multiple sclerosis. Neurobiol. Dis. 21, 626–632.

Kim, J.H., Loy, D.N., Liang, H.F., Trinkaus, K., Schmidt, R.E., and Song, S.K. (2007). Noninvasive diffusion tensor imaging of evolving white matter pathology in a mouse model of acute spinal cord injury. Magn. Reson. Med. 58, 253–260.

Kim, J.H., Tu, T.W., Bayly, P., and Song, S.K. (2009). Impact speed does not determine severity of spinal cord injury in mice with fixed impact displacement. J. Neurotrauma

Kim, T.H., Zollinger, L., Shi, X.F., Rose, J., and Jeong, E.K. (2009). Diffusion tensor imaging of ex vivo cervical spinal cord specimens: The immediate and long-term effects of fixation on diffusivity. Anat. Rec. (Hoboken) 292, 234–241.

Kung, C.C., Peissig, J.J., and Tarr, M.J. (2007). Is region-of-interest overlap comparison a reliable measure of category specificity? J. Cogn. Neurosci. 19, 2019–2034.

Loy, D.N., Kim, J.H., Xie, M., Schmidt, R.E., Trinkaus, K., and Song, S.K. (2007). Diffusion tensor imaging predicts hyperacute spinal cord injury severity. J. Neurotrauma 24, 979–990.

Nevo, U., Hauben, E., Yoles, E., Agranov, E., Akselrod, S., Schwartz, M., and Neeman, M. (2001). Diffusion anisotropy MRI for quantitative assessment of recovery in injured rat spinal cord. Magn. Reson. Med. 45, 1–9.

Schwartz, E.D., and Hackney, D.B. (2003). Diffusion-weighted MRI and the evaluation of spinal cord axonal integrity following injury and treatment. Exp. Neurol. 184, 570–589.

Schwartz, E.D., Chin, C.L., Shumsky, J.S., Jawad, A.F., Brown, B.K., Wehrli, S., Tessler, A., Murray, M., and Hackney, D.B. (2005). Apparent diffusion coefficients in spinal cord transplants and surrounding white matter correlate with degree of axonal dieback after injury in rats. AJNR Am. J. Neuroradiol. 26, 7–18.

Song, S.K., Sun, S.W,. Ju, W.K., Lin, S.J., Cross, A.H., and Neufeld, A.H. (2003). Diffusion tensor imaging detects and differentiates axon and myelin degeneration in mouse optic nerve after retinal ischemia. Neuroimage 20, 1714–1722.

Stejskal, E., and Tanner, J.E. (1965). Spin echoes in the presence of a time-dependent field Gradient J. Chem. Phys. 42, 288–292.

Sun, S.W., Liang, H.F., Cross, A.H., and Song, S.K. (2008). Evolving Wallerian degeneration after transient retinal ischemia in mice characterized by diffusion tensor imaging. Neuroimage 40, 1–10.

Address correspondence to:
Sheng-Kwei Song, Ph.D.
Biomedical MR Laboratory
Campus Box 8227
Washington University School of Medicine
Room 2313, 4525 Scott Avenue
St. Louis, MO 63110

E-mail: ssong@wustl.edu